PERGAMON

International Journal of Solids and Structures 38 (2001) 1855–1870

INTERNATIONAL JOURNAL OF SOLIDS and STRUCTURES

www.elsevier.com/locate/ijsolstr

Three dimensional elastoplastic contact analysis at large strains with enhanced assumed strain elements

Katri I. Ika Ferreira [a], Deane Roehl [b,*]

[a] *Department of Structural Engineering, Federal University of Roraima, UFRR, Brazil*

[b] *Department of Civil Engineering, PUC-RIO, Rua Marques de Sao Vicente, 225 Gavea, 22453-900 Rio de Janeiro, Rio de Janeiro, Brazil*

Received 10 September 1999

Abstract

In this paper, a model for elastoplastic contact analysis under large strain conditions is presented. Consideration of the impenetrability constraints follows through a penalty formulation. Due to the presence of large strains and to the impenetrability restrictions, special care by the choice of the finite element formulation is required. Here, the enhanced assumed strain concept is employed. Since this concept is based on the enhancement of the strain fields with no interelement continuity requirement imposed, the simple global structure of the displacement based model remains unchanged. © 2001 Published by Elsevier Science Ltd. All rights reserved.

Keywords: Contact; Penalty method; Large strains; Elastoplasticity; Enhanced assumed strain elements

1. Introduction

Problems involving multi-body contact are present in many industrial applications, metal forming processes, collision of vehicles, semi-rigid connections in steel structures and problems related to the biomechanics, as for instance the determination of stresses in human joints and implants. In this variety of applications, contact problems combined with large deformations in elastic and plastic regimes require for special formulations to treat on the one hand the impenetrability constraints, and on the other hand to model the inelastic material behavior as well as to account for large deformations in the process.

The mechanical modeling of the interface of contact requires both the introduction of the geometric condition of non-penetration and the development of constitutive laws for the mechanical description of the surface interaction. In some cases, such as metal forming applications, the correct establishment of the geometric restrictions suffices and the surface pressure can be deduced from the contact reactions. The determination of the tangential contact forces due to friction is however a more complex task. Elastoplastic constitutive models based on the Coulomb friction law are often employed, as in the works of Cheng and

* Corresponding author.
E-mail address: droehl@civ.puc-rio.br (D. Roehl).

0020-7683/01/$ - see front matter
PII: S0020-7683(00)00139-6

Kikuchi (1985) and Chaudary and Bathe (1986). Frictional contact response of composed systems under impact loading is addressed by Wriggers et al. (1990) and by Karaoghan and Noor (1995).

For normal contact, the contact conditions are given in the form of inequalities and the solution of the normal contact problem can be formulated as an optimization problem with inequalities as restrictions. This approach has been followed in the works of Bjorkman et al. (1995), where a quadratic minimization problem with inequality constraints is reduced to a linear complementary problem. Joo and Kwak (1986), with emphasis on quadratic recursive programming, analyze elastoplastic contact problems.

Two other approaches, which have received great attention are the Lagrange multiplier method and the penalty method. These methods consist in transforming a minimization problem with inequality restrictions in an unrestricted problem by including the restriction in the functional of the problem. Both methods allow initial violation of the impenetrability constraint and correct it by expulsing the overlapping body regions.

In the penalty method, these restrictions are only approximated, and the quality of the approximation depends strongly on the choice of the penalty parameter. An example of the application of the penalty method is given by Papadopoulos and Taylor (1992), where a hybrid penalty formulation for two dimensional contact is presented. In the work of Rothert et al. (1992) and in a following development of the same authors (Gebbeken et al., 1994), small strain elastoplastic contact problems are solved with the penalty formulation. Application of this method to large strain problems is found in the work of Peric and Owen (1992).

In the Lagrange multiplier method, the inequality constraints are imposed directly to the problem by addition of the contact restrictions as equations to be solved simultaneously with the equilibrium equations, composing a system of non-linear equations in the displacements and contact forces. The Lagrange multiplier method is applied for instance in the work of Bathe and Chaudary (1985) to plane and axisymmetric contact problems with friction and extended by the authors in a following work (1986) to the three-dimensional dynamic analysis of contact. In the works of Simo et al. (1985) and Simo and Laursen (1992), an augmented Lagrangian formulation was employed together with a hybrid finite element formulation, where the normal contact pressure is approximated independently at the contact surface. This formulation is applied to frictionless contact of elastic and elastoplastic bodies in the first work and to problems involving friction in the latter.

In the present work, a methodology for the numerical analysis of three-dimensional elastoplastic frictionless contact problems at large strains is proposed. For the numerical solution procedure including the treatment of both physical and geometrical non-linearities additionally to those arising from contact, an incremental iterative strategy based on the finite element method is employed. For each load increment, the relative position between the bodies is updated and a new contact geometry is established.

For the solution of the contact problem, the penalty method is adopted. The geometry of contact is general, i.e. node to surface contact is considered. In order to simplify the contact geometry and determination of contact forces, linear eight node hexahedral elements were used. The well-known locking effects, present in such elements are diminished through the use of a hybrid formulation, the enhanced assumed strain (EAS) formulation, proposed by Simo and Rifai (1990). Some numerical examples illustrate the applicability of the proposed methodology.

2. The contact problem

2.1. Problem description

The description of motion of two deformable bodies B^i, $i = 1, 2$, which come into contact is shown in Fig. 1. The interior and contour of each body are represented, respectively, by Ω^i and $\partial\Omega^i$. Motion of B^i is

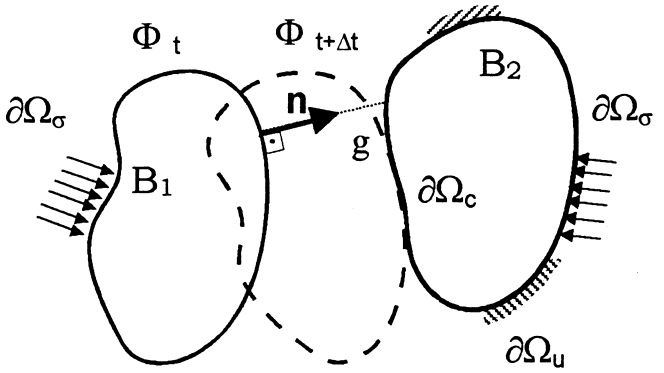

Fig. 1. Contact description.

described by the mapping φ^i in $\Omega^i \cup \partial\Omega^i$, so that the current position vector of a material point P on B^i, which is identified in the reference configuration by coordinates $\mathbf{X}(\mathrm{P})$, is given by

$$\mathbf{x}(\mathrm{P}) = \varphi^i(\mathbf{X}(\mathrm{P}), t) = \varphi^i_t. \tag{2.1}$$

Contact can occur at any arbitrary region of the boundary for which the physical condition of impenetrability must be satisfied. The bodies and their contours in the current configuration are identified through

$$\Omega^i_t := \varphi^i(\Omega^i, t) \quad \text{and} \quad \partial\Omega^i_t := \varphi^i(\partial\Omega^i, t), \tag{2.2}$$

respectively, and the unit normal vectors to each surface $\partial\Omega^i_t$ are described by $\mathbf{n}^i_t$. At time t, the two bodies are supposed in contact along a surface $\partial\Omega_c$, i.e.,

$$\partial\Omega^1_t \cap \partial\Omega^2_t := \partial\Omega_c \neq \varnothing. \tag{2.3}$$

The non-penetration condition is expressed as

$$\Omega^1_t \cap \Omega^2_t = \varnothing. \tag{2.4}$$

Mathematically, condition (2.4) can be formulated with the aid of a scalar configuration dependent differentiable function known as the gap function, which controls the distance between the bodies. This function is defined on the body surfaces $\partial\Omega^i_t$ for each time t as

$$g_t = (\mathbf{x}^2_t - \mathbf{x}^1_t) \cdot \mathbf{n}_t, \tag{2.5}$$

where $\mathbf{x}^1$ and $\mathbf{x}^2$ represent any two position vectors of material points on each body surface. For the gap function, the following conditions hold:

$$g(\mathbf{x}^1, \mathbf{x}^2) = 0 \quad \text{for } \mathbf{x}^1, \mathbf{x}^2 \in \partial\Omega_c, \tag{2.6a}$$

$$g(\mathbf{x}^1, \mathbf{x}^2) > 0 \quad \text{for } \mathbf{x}^1, \mathbf{x}^2 \notin \partial\Omega_c. \tag{2.6b}$$

In the above equations and in what follows, the subscript t identifying the current configuration was omitted for the sake of clarity.

As a consequence of contact, compressive forces arise between the bodies. Consider $\mathbf{t}(\mathbf{x}), \mathbf{x} \in \partial\Omega_c$, the vector field representing the contact forces. Under the hypothesis of frictionless and adhesionless contact, the traction vector field on the contact surface must be normal to the surface and is assumed to be given by the following constitutive equation:

$$\sigma \cdot \mathbf{n} = \mathbf{t} = -\lambda \nabla g \quad \text{on } \partial\Omega_c. \tag{2.7}$$

In this expression, λ is a scalar field representing the contact pressure and the operator ∇g represents the gradient of the gap function with respect to the updated coordinates $\mathbf{x}$. Concisely, the contact conditions described by impenetrability, compressive contact forces and complementarity between contact forces and the gap between the bodies can be expressed in the Kuhn–Tucker complementary form as

$$g_t \geqslant 0, \tag{2.8a}$$

$$\lambda \geqslant 0, \tag{2.8b}$$

$$\lambda g_t = 0. \tag{2.8c}$$

The formulation of the classical weak form of equilibrium restricted to the static case completes the problem description:

$$\int_{\Omega_t} \sigma \colon \operatorname{grad} \delta\mathbf{u}\, \mathrm{d}v - \int_{\Omega_t} \rho\mathbf{b} \cdot \delta\mathbf{u}\, \mathrm{d}v - \int_{\partial\Omega_t} \bar{\mathbf{t}}.\delta\mathbf{u}\, \mathrm{d}s - \int_{\partial\Omega_c} \lambda \nabla g(\mathbf{u}) \cdot \delta\mathbf{u}\, \mathrm{d}s = 0 \tag{2.9}$$

with Cauchy stresses σ, body forces $\mathbf{b}$ and prescribed surface tractions $\bar{\mathbf{t}}$. The last integral represents the work of the contact forces.

2.2. Constitutive framework

The constitutive model considered here is that of finite strain elastoplasticity based on maximum plastic dissipation and on the multiplicative decomposition of the deformation gradient as proposed by Lee (1969):

$$\mathbf{F} = \mathbf{F}_e\mathbf{F}_p, \tag{2.10}$$

Associated with this decomposition is the notion of an unstressed incompatible intermediate configuration which is up to a rotation uniquely defined. Further, we assume the existence of a strain energy function W in the following special form (Simo, 1988a,b):

$$\rho\psi = \left\{ \tfrac{1}{2}\kappa(\ln \mathrm{J})^2 + \tfrac{1}{2}\mu(\mathbf{g} : \bar{\mathbf{b}}_e - 3) \right\} + \rho\psi^{\mathrm{P}}(\bar{\varepsilon}_{\mathrm{P}}). \tag{2.11}$$

In the equation above, $\mathbf{g}$ is the metric tensor, and $\bar{\mathbf{b}}_e$ is the modified elastic left Cauchy–Green tensor defined on the intermediate configuration:

$$\bar{\mathbf{b}}_e := \bar{\mathbf{F}}_e\bar{\mathbf{F}}_e^{\mathrm{T}} = \mathrm{J}^{2/3}\mathbf{F}_e\mathbf{F}_e^{\mathrm{T}} = \mathrm{J}^{2/3}\mathbf{b}_e, \tag{2.12}$$

where

$$\mathbf{F} = \mathrm{J}^{1/3}\bar{\mathbf{F}} \quad \text{and } \det \bar{\mathbf{F}} = 1. \tag{2.13}$$

Considering $J2$ flow theory with isotropic hardening, the governing equations of the rate independent associative elastoplastic problem are summarized as follows:

$$\phi = \phi(\mathbf{g}, \mathbf{s}, \bar{\varepsilon}_{\mathrm{P}}) = \|\mathrm{a}\| - \sqrt{\tfrac{2}{3}}\sigma_{\mathrm{y}}(\bar{\varepsilon}_{\mathrm{P}}) \quad \text{(yield surface)}, \tag{2.14}$$

$$L_{\mathrm{v}}\tau = \dot{\gamma}\frac{\partial\phi}{\partial\mathbf{g}} = 2\bar{\mu}\dot{\gamma}\frac{\mathbf{s}}{\|\mathbf{s}\|} \quad \text{(associated flow rule)}, \tag{2.15}$$

$$\dot{\bar{\varepsilon}}_{\mathrm{P}} = \dot{\gamma}\sqrt{\tfrac{2}{3}} \quad \text{(evolution of the hardening parameter)}. \tag{2.16}$$

In the above equations, the stress deviator $\mathbf{s}$ is defined as

$$\mathbf{s} = \operatorname{dev}\tau = \mu(\bar{\mathbf{b}}_e - \tfrac{1}{3}(\bar{\mathbf{b}}_e : \mathbf{g})\mathbf{g}^{-1}) \tag{2.17}$$

with $\bar{\mu} = \frac{1}{3}\mu\mathbf{J}^{2/3}\operatorname{tr}\bar{\mathbf{b}}_e$, $\dot{\gamma}$ is the plastic multiplier which satisfies the loading/unloading (Kuhn–Tucker) conditions.

$$\dot{\gamma} \geqslant 0, \quad \phi(\mathbf{g}, \mathbf{b}_e^{-1}, \mathbf{q}) \leqslant 0, \quad \dot{\gamma}\phi = 0. \tag{2.18}$$

3. Discrete incremental problem

3.1. Incremental equilibrium

The numerical solution of the non-linear system of Eqs. (2.9) is obtained iteratively through the Newton method considering an incremental description of motion in the current configuration. An important aspect of this methodology is the consistent linearization of the cinematic, equilibrium equations and constitutive relations in order to assure the quadratic rate of convergence of the Newton method.

The independent variables, displacement and contact forces, at configuration $n+1$ are determined by

$$\mathbf{u}_{n+1} = \mathbf{u}_n + \Delta\mathbf{u}_{n+1}, \tag{3.1}$$

$$\lambda_{n+1} = \lambda_n + \Delta\lambda_{n+1}. \tag{3.2}$$

The incremental form of the impenetrability condition is given by

$$g_{n+1} = (\mathbf{x}^2_{n+1} - \mathbf{x}^1_{n+1}) \cdot \mathbf{n}_{n+1}, \quad g_{n+1} \geqslant 0, \tag{3.3}$$

and the virtual work is expressed for the current configuration as

$$\delta w_{n+1} = \int_\Omega \sigma_{n+1} : \operatorname{grad}\delta\mathbf{u}\,dv - \int_\Omega \rho\mathbf{b}_{n+1}\cdot\delta\mathbf{u}\,dv - \int_{\partial\Omega} \bar{\mathbf{t}}_{n+1}\cdot\delta\mathbf{u}\,ds - \int_{\partial\Omega_c} \lambda_{n+1}\nabla g_{n+1}(\mathbf{u})\cdot\delta\mathbf{u}\,ds = 0. \tag{3.4}$$

With the following linear approximations for g_{n+1} and σ_{n+1},

$$L(g_{n+1}) = g_n + \nabla\mathbf{g}_n(\mathbf{u}_n)\cdot(\mathbf{u}_{n+1} - \mathbf{u}_n) = g_n + \nabla\mathbf{g}_n\cdot\Delta\mathbf{u}_{n+1}, \tag{3.5}$$

$$L(\sigma_{n+1}) = \sigma^*_n + \Delta\sigma_{n+1} = \sigma^*_n + \mathbf{c}^{ep} : \operatorname{grad}^s\Delta\mathbf{u}_{n+1}, \tag{3.6}$$

the incremental linearized form of the virtual work follows whereby the quadratic terms were dropped. In the above equation, the expressions grad^s and ∇ denote respectively, the symmetric gradient with respect to the updated coordinates, and the derivatives with respect to the displacements.

$$\int_{\Omega_t} (\operatorname{grad}^s\Delta\mathbf{u}_{n+1} : \mathbf{c}^{ep}_n : \operatorname{grad}\delta\mathbf{u} + \operatorname{grad}\Delta\mathbf{u}_{n+1} : \sigma_n : \operatorname{grad}\delta\mathbf{u})\,dv - \int_{Sc} (\lambda_n\nabla g_n + \Delta\lambda_{n+1}\nabla g_n + \lambda_n\nabla^2 g_n : \Delta\mathbf{u}_{n+1}) \cdot\delta\mathbf{u}\,ds = \int_{\Omega_t} \rho\mathbf{b}_{n+1}\cdot\delta\mathbf{u}\,dv + \int_{s_t} \bar{\mathbf{t}}_{n+1}\cdot\delta\mathbf{u}\,dv - \int_{\Omega_t} \sigma_n : \operatorname{grad}\delta\mathbf{u}\,dv. \tag{3.7}$$

Considering the presence of large deformations, the initial stress tensor σ_n has to be updated to the current configuration $n+1$, as given by the following expression:

$$\sigma^*_n = \frac{1}{\Delta J}\Delta\mathbf{F} : \sigma_n : \Delta\mathbf{F}^T,$$

where

$$\Delta\mathbf{F} = \partial\mathbf{x}_{n+1}/\partial\mathbf{x}_n \quad \text{and} \quad \Delta J = \det\Delta\mathbf{F}. \tag{3.8}$$

In the above development, the inelastic character of the material is present through the consistent elastoplastic material tensor $\mathbf{c}_{ep}$ (Simo, 1988a, b) according to the constitutive model presented in Section 2.

3.2. Solution of the contact problem

In this work, the contact conditions will be satisfied approximately by the use of a penalty formulation. The penalty method was also used by other authors to approximate the impenetrability constraint (Papadopoulos et al., 1995; Saracibar, 1997). In this formulation, the contact pressure will be approximated by the constitutive relation:

$$\lambda = \beta\langle - g(\mathbf{u})\rangle, \tag{3.9}$$

where β is the positive a penalty parameter. Once the contact forces must be non-negative, satisfaction of the above equation implies in negative values for the gap function, i.e., violation of the impenetrability constraint. In this case, the bodies penetrate each other partially and are pulled apart again by the contact forces during the equilibrium iterations. In this way, in an iterative procedure, the penetration is to removed an acceptable extent. The tolerance for the penetration will depend on the physical problem considered. Substitution of Eq. (3.8) for λ_{n+1} in the virtual work expression (3.7) leads to the following linearized form:

$$\begin{aligned}\int_{\Omega_t} (\mathrm{grad}^{\mathrm{s}}\,\Delta\mathbf{u}_{n+1} : \mathbf{c}_n^{\mathrm{ep}}\colon \mathrm{grad}\,\delta\mathbf{u} + \mathrm{grad}\,\Delta\mathbf{u}_{n+1} : \sigma_n\colon \mathrm{grad}\,\delta\mathbf{u})\,\mathrm{d}v + \int_{\partial\Omega_c} \beta(\nabla g_n \otimes \nabla g_n + \mathrm{g}_n \nabla^2 g_n) \\ \cdot\,\Delta\mathbf{u}_{n+1}\cdot\delta\mathbf{u}\,\mathrm{d}s = \int_{\Omega_t} \rho\mathbf{b}_{n+1}\cdot\delta\mathbf{u}\,\mathrm{d}v + \int_{\partial\Omega_t} \bar{\mathbf{t}}_{n+1}\cdot\delta\mathbf{u}\,\mathrm{d}v - \int_{\Omega_t} \sigma_n\colon \mathrm{grad}\,\delta\mathbf{u}\,\mathrm{d}v - \int_{\partial\Omega_c} \beta \mathrm{g}_n \nabla g_n\cdot\delta\mathbf{u}\,\mathrm{d}s.\end{aligned} \tag{3.10}$$

4. Finite element discretization

4.1. Discrete contact geometry

Historically linear kinematics assuming node to node contact was first investigated. However, in the case of large deformation analysis, node to node contact cannot be presupposed and contact kinematics becomes much more complicated.

Fig. 2 shows the contact of two generic bodies which are arbitrarily denoted as *contactor* and *target*. In the finite element solution, the contactor contains the boundary nodes which will come into contact with the target surface, segments or nodes of the target body. The basic condition of contact along the a priori unknown contact region is that no material overlap can occur. Due to contact, equal and opposite compressive forces develop on the contact surface. Since tangential tractions are not considered here, the total stress vector at contact must be perpendicular to the contact area.

The geometric relations for contact detection for a three-dimensional problem are explained in Fig. 2 (Rothert et al., 1992). The surfaces of the contacting bodies are discretized using quadrilateral surface segments. For this discretization, the distance function g_P is introduced which controls the distance from the contactor node P to the target body. Considering an element of the target contact surface defined by a plane including nodal points A, B and C, its unit normal vector can be determined through the vector product $\mathbf{b}\times\mathbf{c}$. Contact of a generic nodal point P with this surface element is then only possible if the projection of P along the direction $\mathbf{n}$ falls within the surface element ABC. From the definition of the discrete gap function, it is clear that this function depends on the coordinates of nodal points A, B, C and P, which are updated at each Newton–Raphson iteration along with the surface normal $\mathbf{n}$. It is worth men-

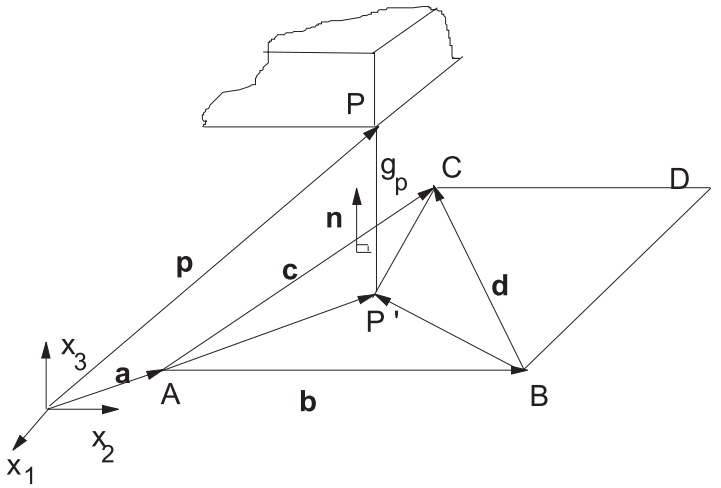

Fig. 2. Discrete contact geometry.

tioning that in this procedure, the list of potential contact nodes is established at the beginning of each incremental step. Therefore, changes of contact surface elements within a load step are not considered:

$$g_{\mathrm{P}} = \left(\mathbf{x}^{\mathrm{P}} - \mathbf{x}^{\mathrm{A}}\right) \cdot \mathbf{n} = \left(\mathbf{x}^{\mathrm{P}} - \mathbf{x}^{\mathrm{A}}\right) \cdot \frac{\mathbf{h}}{\|\mathbf{h}\|} = \frac{q}{\|\mathbf{h}\|} \quad \text{with} \quad \mathbf{n} = \frac{\mathbf{b} \otimes \mathbf{c}}{\|\mathbf{b} \otimes \mathbf{c}\|} = \frac{\mathbf{h}}{\|\mathbf{h}\|}. \tag{4.1}$$

4.2. Discrete equilibrium

Considering a displacement based finite element formulation after integration of Eq. (3.9), the following discrete equilibrium equation is obtained:

$$[\mathbf{K}(\mathbf{d}) + \mathbf{K}_{\mathrm{c}}(\mathbf{d}_{\mathrm{c}})]_n \Delta \mathbf{d}_{n+1} = \mathbf{R}_{n+1} - \mathbf{f}_n(\mathbf{d}) - \mathbf{f}_{\mathrm{c}_n}(\mathbf{d}_{\mathrm{c}}). \tag{4.2}$$

The displacements of the nodes present at contact at time n are arranged in $\mathbf{d}_{\mathrm{c}}$, being part of the global displacement vector $\mathbf{d}$. The matrix $[\mathbf{K} + \mathbf{K}_{\mathrm{c}}]$ corresponds to the global consistent tangent stiffness (Wriggers and Simo, 1985), and the right-hand side to the unbalanced forces, whereby $\mathbf{R}$ is the external load vector, $\mathbf{f}$ is the vector of internal forces and $\mathbf{f}_{\mathrm{c}}$ is the vector of contact forces. The matrices and vectors present in Eq. (4.2) are defined as follows:

$$\mathbf{K}_{\mathrm{c}}(\mathbf{d}_{\mathrm{c}}) = \bigcup_{j=1}^{n_{\mathrm{c}}} \beta(\nabla \mathbf{g}_j^{\mathrm{T}} \nabla \mathbf{g}_j + \mathbf{g}_j^{\mathrm{T}} \nabla^2 \mathbf{g}_j), \tag{4.3}$$

$$\mathbf{f}_{\mathrm{c}}(\mathbf{d}_{\mathrm{c}}) = \bigcup_{j=1}^{n_{\mathrm{c}}} \beta \mathbf{g}_j^{\mathrm{T}} \nabla \mathbf{g}_j, \tag{4.4}$$

$$\mathbf{f}(\mathbf{d}) = \bigcup_{e=1}^{n_{\mathrm{el}}} \int_{\Omega_t} \mathbf{B}^{\mathrm{T}} \sigma \, \mathrm{d}v^e, \tag{4.5}$$

$$\mathbf{K}(\mathbf{d}) = \bigcup_{e=1}^{n_{\mathrm{el}}} \int_{\Omega_t} (\mathbf{B}^{\mathrm{T}} \mathbf{c}^{\mathrm{ep}} \mathbf{B} + \mathbf{B}_{\mathrm{G}}^{\mathrm{T}} \sigma \mathbf{B}_{\mathrm{G}}) \mathrm{d}v^e, \tag{4.6}$$

where n_{el} is the number of finite elements and matrices $\mathbf{B}$ and $\mathbf{B}_G$ contain the form function derivatives for the integration of the material and geometrical stiffness matrices respectively. It is worth mentioning that in this work, the gap function is evaluated directly at the contact nodes.

The determination of the contact matrix $\mathbf{K}_c$ which is consistent with the application of the classical Newton method is derived in the work of Parisch (1989) and presented shortly here. For the discrete form of the gap function given by Eq. (4.1), the first and second derivatives of this function with respect to the current nodal coordinates of nodes A, B, C and P (Fig. 2) are given, respectively, by

$$\frac{\partial g}{\partial d_k^I} = \left(\frac{\partial q}{\partial d_k^I} \|\mathbf{h}\|^2 - \frac{\partial \|\mathbf{h}\|^2}{2\partial d_k^I} \mathrm{q} \right) \Big/ \|\mathbf{h}\|^3, \quad I = \mathrm{A,B,C,P}, \;\; k = 1,2,3, \tag{4.7}$$

$$\frac{\partial^2 g}{\partial d_k^I \partial d_l^J} = \left[\left(\frac{\partial^2 q}{\partial d_k^I \partial d_I^J} \|\mathbf{h}\|^2 - \frac{\partial q \partial \|\mathbf{h}\|^2}{2\partial d_k^I \partial d_I^J} - \frac{\partial q \partial \|\mathbf{h}\|^2}{2\partial d_I^I \partial d_k^J} - \frac{\partial^2 \|\mathbf{h}\|^2}{2\partial d_k^I \partial d_l^J} \mathrm{q} \right) \|\mathbf{h}\|^2 + \frac{3\partial \|\mathbf{h}\|^2 \partial \|\mathbf{h}\|^2}{4\partial d_k^I \partial d_l^J} \mathrm{q} \right] \Big/ \|\mathbf{h}\|^5,$$
$$I,J = \mathrm{A,B,C,P}, \;\; k,l = 1,2,3. \tag{4.8}$$

For each contact node P of the contactor body, Eq. (4.7) results in a vector with 12 components and Eq. (4.8) in a square matrix with 12 rows and columns, which are to be assembled in the global matrix $\mathbf{K}_c$.

4.3. Enhanced assumed strain formulation

In order to avoid the deficiencies inherent to a displacement based finite element formulation, the EAS hybrid formulation, proposed by Simo and Rifai (1990) will be employed here. In this formulation, the compatible deformation field is enriched through an additional one, in such a way to diminish the well known spurious locking of the finite element model. This effect is specially presented by low order elements. Considering the analysis of large deformation elastoplastic contact problems, these effects are even more critical. The EAS formulation was extended for large strain kinematics in the work of Simo and Armero (1992) and improved in the following work of Simo et al. (1993). Its efficiency and reliability for the calculation of large elastoplastic strains has been also verified in the work of Roehl and Ramm (1996). An extension of the applicability of these elements to the contact analysis with the penalty method is the aim of this section.

The EAS formulation is based on the three-field Hu–Washizu functional, by which the deformation field is enhanced through additional functions, chosen in such a way to improve element performance and to guarantee convergence and stability (Simo et al., 1993). In the EAS formulation for large strains, an enhancement of the deformation field is obtained through incompatible functions for the deformation gradient $\tilde{\mathbf{F}}$:

$$\tilde{\mathbf{F}} = \mathbf{F}_\phi + \tilde{\mathbf{H}} = 1 + \mathrm{grad}\,\mathbf{u} + \tilde{\mathbf{H}}, \tag{4.9}$$

in which $\mathrm{grad}\,\mathbf{u} = \mathbf{Bu}$ contains the compatible deformations and $\tilde{\mathbf{H}} = \tilde{\mathbf{B}}\alpha$ the enhancement of the deformation field. Since no interelement continuity is required for the deformation fields, the internal strain parameters α are eliminated at element level, and the simple structure of the displacement model is preserved. Further developments on EAS elements are found by Simo et al. (1993) and Roehl and Ramm (1996). Integration of the virtual work expression with the above assumptions results in the equilibrium equations:

$$\left[\tilde{\mathbf{K}} + \mathbf{K}_c \right]_n \Delta \mathbf{u}_{n+1} = \mathbf{R}_{n+1} - \mathbf{f}_n - \mathbf{f}_{c_n}, \tag{4.10}$$

where $\tilde{\mathbf{K}}$ is the consistent elastoplastic stiffness matrix obtained with the enhanced deformation gradient $\tilde{\mathbf{F}}$. As can be seen from Eq. (4.10), the introduction of the enhanced deformation terms does not modify the structure of the equilibrium equation.

5. Numerical examples

In the following examples, large deformations in *J*2 elastoplasticity is considered. Details of the large strain plasticity constitutive model can be taken from Roehl and Ramm (1996). Results obtained with linear displacement elements (Hexa8) are compared with EAS elements, by which a complete tri-linear interpolation is employed (Hexa8-E3). While considering a linear hexahedral element (eight nodes), this implies nine internal strain parameters (Roehl and Ramm, 1996).

5.1. Contact of two cantilever slabs

This example is based on the work of Binder and Gebbeken (1992), wherein the three-dimensional problem of the contact between two unsymmetrically loaded cantilever beams is analyzed with a mesh of 20-node hexahedral elements. von Mises' criterion for yielding with isotropic hardening according to the following exponential function is employed:

$$\sigma_y(\bar{\varepsilon}_P) = y_1 + (y_2 - y_1)(1 - e^{(y_3\bar{\varepsilon}_P)}) + y_4\bar{\varepsilon}_P \ (\mathrm{kN/cm^2}),$$

where $y_1 = 24.0$, $y_2 = 20.2$, $y_3 = 30.0$ and $y_4 = 93.2$. The elasticity modulus is $E = 21\,000.0$ kN/cm^2, Poisson's ratio is $v = 0.3$ and the applied loads are $F_1 = 90$ kN, $F_2 = 60$ kN and $F_3 = 30$ kN.

The geometry and the finite element mesh are given in Fig. 3. The diagram shown in Fig. 4 compares the load–displacement curves at point A for the EAS element mesh (Hexa8-E3) obtained in the present work and those obtained with the 20-node hexahedra (Hexa20) according to Binder and Gebbeken (1992), showing a small deviation of the results. The present analysis was carried out further than the reference

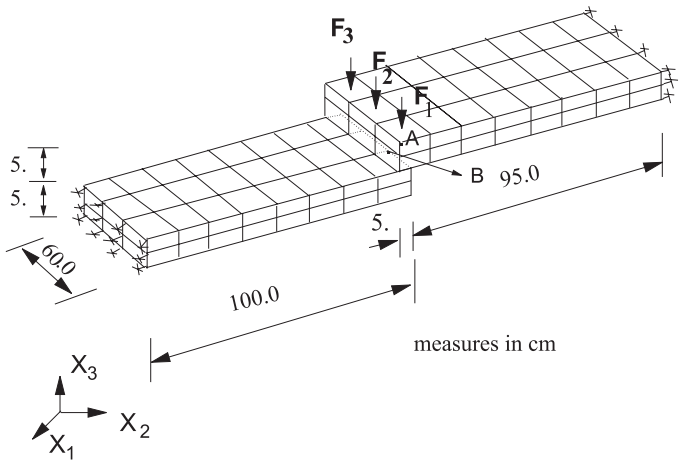

Fig. 3. Contact of two cantilever slabs: geometry and model discretization.

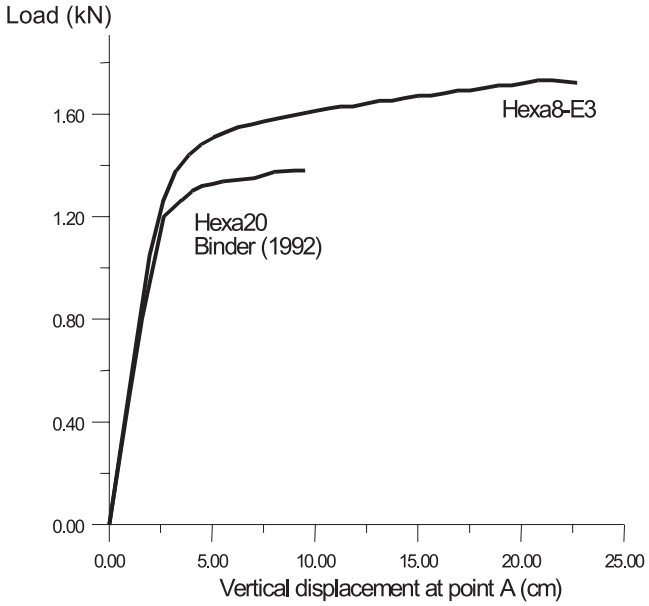

Fig. 4. Contact of two cantilever slabs: load–displacement curves.

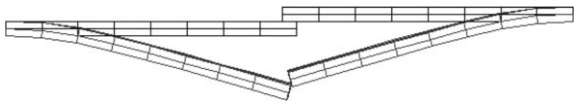

Fig. 5. Contact of two cantilever slabs: deformed configuration.

results, being able to reproduce the complete loading history until loss of contact. Fig. 5 depicts the deformed configuration at final stage of loading.

5.2. Endplate connection

The second example was taken from Gebbeken et al. (1994) and Rothert et al. (1992). In this example, the semi-rigid behavior of an extended endplate connection is studied. This analysis focuses on the tension area of the column web and flange, which is connected to the beam through the endplate (Fig. 6). It is assumed that the endplate is rigid compared with the column flange thickness. Loads are applied in column web plane (plane xz) and the boundary conditions are such that no out-of-plane displacements are allowed.

Due to symmetry considerations, only an eighth of the connection is modeled. Fig. 7 shows a detail of the connection. For all plates, ST37 was employed, with the following material properties: elasticity modulus $E = 2.1 \times 10^8$ kN/m^2, yield stress $\sigma_y = 2.4 \times 10^5$ kN/m^2. For the bolts, the yield stress is $\sigma_y = 10 \times 10^5$ kN/m^2. Some additional hypotheses are made: geometry of the screw is considered in a simplified way and its thread is not considered; perfect adhesion between column flange and bolt head is considered and friction between column flange and endplate is not present. Loads are applied as nodal forces to the column web. A constant penalty parameter $\beta = 10^3$ was employed throughout the analysis.

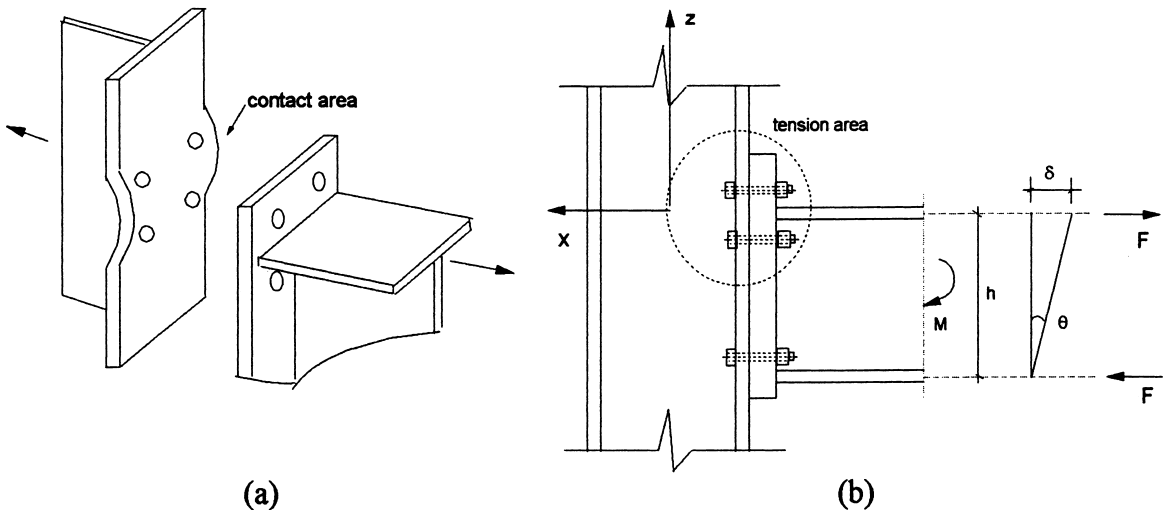

Fig. 6. Endplate connection: (a) detail of contact zone; and (b) loading plane.

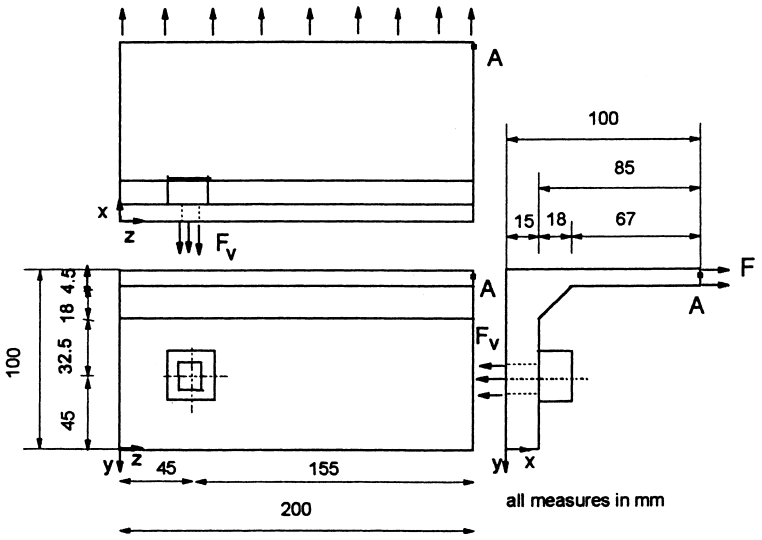

Fig. 7. Endplate connection: detail of the column.

The numerical results with EAS elements and experimental results are shown in Fig. 8, where a good agreement is observed. The deformed configuration at final stage is given in Fig. 9.

5.3. Pinching of pipe by two flexible plates

This last example was taken from Saracibar (1997), wherein large deformation elastoplastic problems with friction are studied. The example consists of an aluminum pipe, which is pinched by a pair of flexible

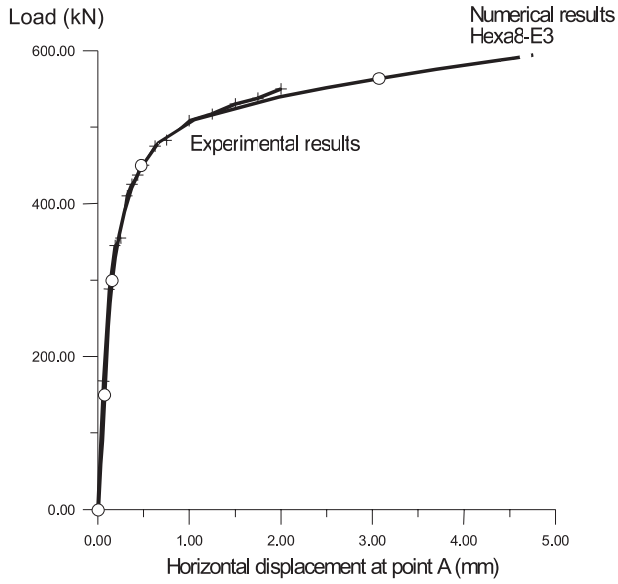

Fig. 8. Endplate connection: load–displacement curves.

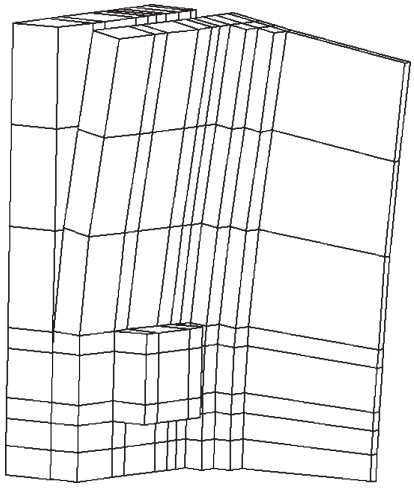

Fig. 9. Endplate connection: deformed configuration.

aluminum plates. The material properties for both pipe and plates are: bulk modulus $K = 74.4$ GPa, shear modulus $G = 28.5$ GPa and yield stress $\sigma_y = 485$ MPa. Ideal plasticity is assumed. The pipe dimensions are: internal radius of 9 cm, outer radius of 10 cm and length of 40 cm. The plates are 2 cm thick, 40 cm long and 15 cm wide. Here, no friction between plates and pipe was considered. Due to symmetry, one eighth of the geometry was modeled. For the discretization 128 continuum elements were used for the pipe and 32 continuum elements for the plate, as shown in Fig. 10. Analysis with both the displacement based model and EAS elements were carried out. The analysis followed displacement controlled, by imposing vertical displacements to point A in steps of 0.1 cm with a constant value of the penalty parameter $\beta = 10^3$. The

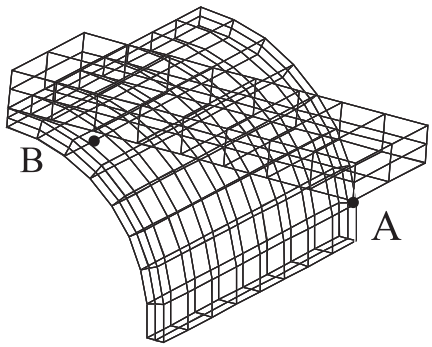

Fig. 10. Pinching of pipe by two flexible plates: model discretization.

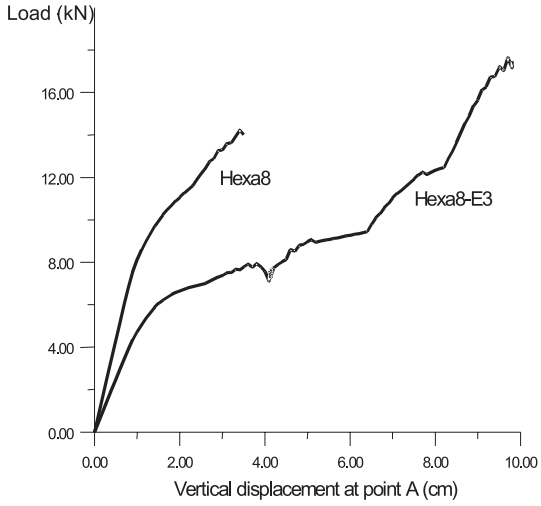

Fig. 11. Load–displacement curve with $\beta = 10^4$.

load–displacement diagram of Fig. 11 confirms the superiority of the EAS model (Hexa8-E3), whereby the displacement based model, not only presented far to stiff results, but was also unable to accomplish the analysis.

In this example, the influence of the penalty parameter on the quality of the results is also investigated. Although higher values for this parameter lead to better satisfaction of the impenetrability constraints, values that are too high cause oscillations of the solution and even interrupt the analysis. In structures with non-linear behavior, the optimal value for the penalty parameter will vary throughout the analysis according to the variation of the stiffness. In this example, the analysis was started with a value of $\beta = 10^{10}$ and as the convergence rate decreased, successive reductions of β of a factor 10 were applied. The load–displacement curve for the vertical displacement of node A is depicted in Fig. 12. For large elastoplastic strains, a value of $\beta = 10^3$ was required for convergence. The results were in very close agreement with the first analysis. The lower value $\beta = 10^3$ eliminates the zigzag present in the first analysis and also presents better convergence. Fig. 13 shows the deformed configuration at the final stage of deformation along with the von Mises stresses for each model.

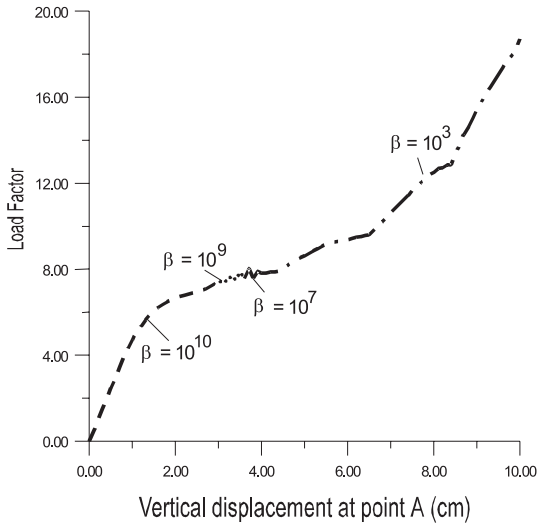

Fig. 12. Load–displacement curve with variable β.

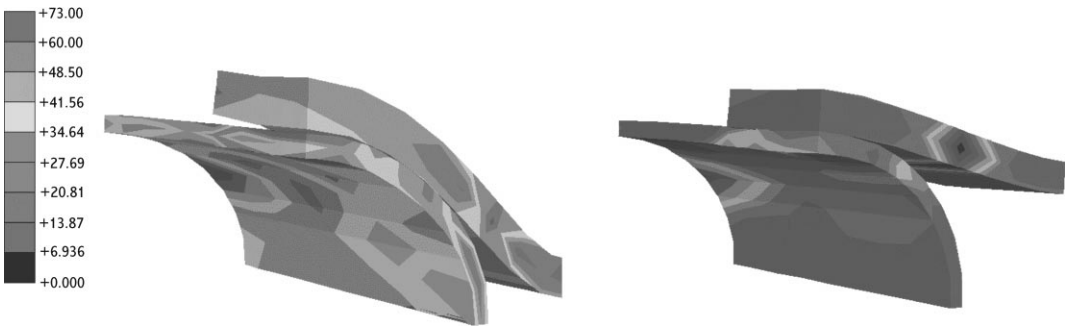

Fig. 13. Pinching of pipe by two flexible plates: von Mises' stresses at the final stage of deformation: (a) EAS (Hexa8-E3) and (b) linear displacement element (Hexa8).

6. Conclusion

In this work, a methodology for the numerical analysis of three dimensional elastoplastic contact problems in the presence of large strains is presented. The methodology is based on the penalty method and the use of EAS elements and was applied to the solution of isothermal problems under frictionless contact conditions. An advantage of this methodology is its easy implementation, whereas both the solution strategy of contact and the hybrid element formulation do not change the global structure and equations of the problem.

The choice of adequate values for the penalty parameter is a well known drawback of the penalty method, but has not been a problem in the examples under study. The results obtained with different values for this parameter were generally in good agreement. Also the EAS elements, although not specially de-

veloped for contact problems, eliminate the locking effects present in the displacement elements and proved to be adequate for contact analysis. Quadratic rate of convergence of the Newton method, due to the employment of the consistent tangent matrix, was observed.

Acknowledgements

The present study is partially supported by research grants of the Brazilian Research Agencies CNPq and FAPERJ. This support is gratefully acknowledged.

References

Bathe, K.J, Chaudhary, A., 1985. A solution method for planar and axisymmetric contact problems. Int. J. Numer. Meth. Engng. 21, 65–88.

Binder, B., Gebbeken, N., 1992. Theoretical and numerical aspects of 3-D finite element elastoplastic-contact analysis. In: Owen, D.R.J., Hinton, E.E., Onate, E. (Eds.), Proceedings of COMPLAS III, Pineridge Press, Swansea.

Bjorkman, G., Klarbing, A., Sjodin, B., 1995. Sequential quadratic programming for non-linear elastic contact problems. Int. J. Numer. Meth. Engng. 38, 137–165.

Chaudhary, A.B., Bathe, K.J., 1986. A solution method for static and dynamic analysis of three-dimensional contact problems with friction. Comput. Struct. 24 (6), 855–873.

Cheng, J.H., Kikuchi, N., 1985. An incremental constitutive relation of unilateral contact with friction for large deformation analysis. J. Appl. Meth. 52, 639–648.

Gebbeken, N., Rothert, H., Binder, B., 1994. On the numerical analysis of endplate connections. J. Construct. Steel Res. 30, 177–196.

Joo, J.W., Kwak, B.M., 1986. Analysis and applications of elasto-plastic contact problems considering large deformation. Comput. Struct. 24 (6), 953–961.

Karaoglan, L., Noor, A.K., 1995. Dynamic sensitivity analysis of frictional contact impact response of axisymmetric composite structures. Comp. Meth. Appl. Mech. Engng. 128, 169–190.

Lee, E.H., 1969. Elastic–plastic deformation at finite strains. J. Appl. Mech. 36, 1–6.

Papadopoulos, P., Taylor, R., 1992. A mixed formulation for the finite element solution of contact problems. Comp. Meth. Appl. Mech. Engng. 94, 373–389.

Papadopoulos, P., Jones, R.E., Solberg, J.M., 1995. A novel finite element formulation for frictionless contact problems. Int. J. Numer. Meth. Engng. 38, 2603–2617.

Parisch, H., 1989. A consistent tangent stiffness matrix for three-dimensional non-linear contact analysis. Int. J. Numer. Meth. Engng. 28, 1803–1812.

Peric, D., Owen, D.R.J., 1992. Computational model for 3-D contact problems with friction based on the penalty method. Int. J. Numer. Methods Engng., 35, 1289–1309.

Saracibar, C.A., 1997. A new frictional time integration algorithm for large slip multi-body frictional contact problems. Comp. Meth. Appl. Mech. Engng. 142, 303–334.

Simo, J.C., Wriggers, P., Taylor, R.L., 1985. A perturbed lagrangian formulation for the finite element solution of contact problems. Comp. Meth. Appl. Mech. Engng. 50, 163–180.

Simo, J.C., 1988a. A framework for finite strain elasto-plasticity based on maximum plastic dissipation and the multiplicative decomposition. Part I. Continuum formulation. Comp. Meth. Appl. Mech. Engng. 66, 199–219.

Simo, J.C., 1988b. A framework for finite strain elastoplasticity based on maximum plastic dissipation and the multiplicative decomposition. Part II. Computational aspects.. Comp. Meth. Appl. Mech. Engng. 68, 1–31.

Simo, J.C., Armero, F., 1992. Geometrically non-linear enhanced strain mixed methods and the method of incompatible modes. Int. J. Numer. Methods Eng. 33, 1413–1449.

Simo, J.C., Armero, F., Taylor, R.L., 1993. Improved versions of assumed enhanced strain tri-linear elements for 3D finite deformation problems. Comp. Meth. Appl. Mech. Eng. 110, 359–386.

Simo, J.C., Laursen, T.A., 1992. An augmented lagrangian treatment of contact problems involving friction. Comput. Struct. 24 (1), 97–116.

Simo, J.C., Rifai, M.S., 1990. A class of assumed strain methods and the method of incompatible modes. Int. J. Numer. Meth. Engng. 29, 1595–1638.

Roehl, D., Ramm, E., 1996. Large elasto-plastic finite element analysis of solids and shells with the enhanced assumed strain concept. Int. J. Solids Struct. 33, 3215–3237.

Rothert, H., Gebbeken, N., Binder, B., 1992. Non-linear three-dimensional finite element contact analysis of bolted connections in steel frames. Int. J. Numer. Meth. Engng. 34, 303–318.

Wriggers, P., Simo, J.C., 1985. A note on tangent stiffness for fully nonlinear contact problems. Commun. Appl. Numer. Meth. 1, 199–203.

Wriggers, P., Van, T., Stein, E., 1990. Finite element formulation of large deformation impact–contact problems with friction. Comput. Struct. 37, 319–331.